

# Influence of Zr-substitution on phase transitions character in polycrystalline $\text{Ba}(\text{Ti}_{1-x}\text{Zr}_x)\text{O}_3$

C. Kajtoch

Received: 27 May 2010 / Accepted: 22 September 2010 / Published online: 5 October 2010  
© The Author(s) 2010. This article is published with open access at Springerlink.com

**Abstract** The results of X-ray diffraction, scanning electron microscopy, and dielectric measurements performed for polycrystalline  $\text{Ba}(\text{Ti}_{1-x}\text{Zr}_x)\text{O}_3$  are presented. Data from these measurements show a change of the type of paraelectric–ferroelectric (PE–FE) phase transition (PT) from sharp PT ( $x < 0.10$ ), through diffuse phase transition ( $0.10 \leq x \leq 0.20$ ), to relaxor type one ( $x = 0.30$ ). The lack of structural PT at the temperature  $T_m$  (the temperature of the maximum of real part of the electric permittivity  $\epsilon'$ ) for  $0.10 \leq x \leq 0.30$ , suggest that this PE–FE transition is not connected with the change of crystal structure. A phase angle of about  $\Phi \approx -90^\circ$ , between electric current and applied voltage, suggests the occurrence of polar regions (clusters) below 400 K. The change of these clusters polarizability and their lability at the  $T_m$  is postulated as possible origin of the observed maximum of  $\epsilon'$ .

## Introduction

The solid solution  $\text{Ba}(\text{Ti}_{1-x}\text{Zr}_x)\text{O}_3$  (BTZx) is the ferroelectric material of perovskite type;  $\text{A}(\text{B}'\text{B}'')\text{O}_3$ . The pure barium titanate (BT) forms four structural phases [1]. At high temperatures (in the paraelectric phase) it has a cubic structure. During decrease of the temperature in BT sample three phase transitions (PT) take place: first to tetragonal phase, T ( $\sim 400$  K), then to rhombic phase, O ( $\sim 300$  K) and finally to rhombohedral phase, R ( $\sim 210$  K). Synthesis conditions [2, 3], piezoelectric [4–6]

and dielectric investigations [7–12] of solid solution BTZx can be found in the literature.

The Ti and Zr ions have the similar configuration of external orbitals (Ti:  $3s^23p^63d^24s^2$ , Zr:  $4s^24p^64d^25s^2$ ) and different radius of ion orbitals (Ti: 68 pm, Zr: 80 pm). This similarity results in regular changes of physical properties of modified materials for different distribution of Zr ions. Statistical distribution of B' and B'' ions cause broadening of the PT temperature region. This fact can be of essential importance in practical applications. BT and BTZx are used as multilayer capacitor ceramics, piezoelectric transducers, PTRC thermistors, and chemical sensors [13–15]. Zirconium titanate (ZT) is used in varistor and tunable microwave filters and as the technical ceramic component [14, 16, 17].

There are two aims of this work. The first is to determine the influence of Zr substitution on the dielectric properties of BTZx. The second is to analyze the change of the character of the paraelectric–ferroelectric (PE–FE) PT (from sharp or DPT to relaxor or glass-type behaviour [18–23]) in this material.

The lack of the structural phase transition at  $T_m$  for  $x \geq 0.10$  suggests that the cause of maximum of  $\epsilon'$  is the change of clusters system polarizability.

## Experimental

The polycrystalline BTZx samples were obtained by the calcination method in two sintering processes at temperatures:  $\sim 1320$  and  $\sim 1620$  K.

The XRD data were collected by Philips X'Pert Pro MD powder diffractometer using  $\text{K}\alpha_1$  radiation from Cu anode. The configuration was standard Bragg–Brentano setup with Ge (111) monochromator at the incident beam. All

C. Kajtoch (✉)  
Institute of Physics, Pedagogical University, Podchorążych 2,  
30-084 Kraków, Poland  
e-mail: ckajtoch@ap.krakow.pl

measurements were performed with the  $0.008^\circ$  step size at  $15^\circ$ – $90^\circ$  scanning range and the 285 s of measurement time for each angle step. The full pattern fitting procedure for quantitative analysis and structural parameters determining was carried out using Philips X'Pert HighScore Plus (PW3212) Release 2.1 software.

The micro-structure of BTZx was investigated by means of a Philips SEM 525 M electron microscope at room temperature.

A sample of the diameter 10 mm and thickness 1.5 mm was covered by silver paint electrodes. The dielectric measurements were performed automatically (QUATRO KRIO 4.0 with LCR Agilent 4824A meter and BDS 1100 cryostat). The measurements were made during cooling at a rate of 2 K/min, within the frequency range of 20 Hz–1 MHz.

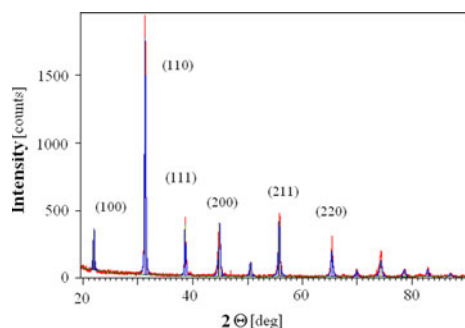
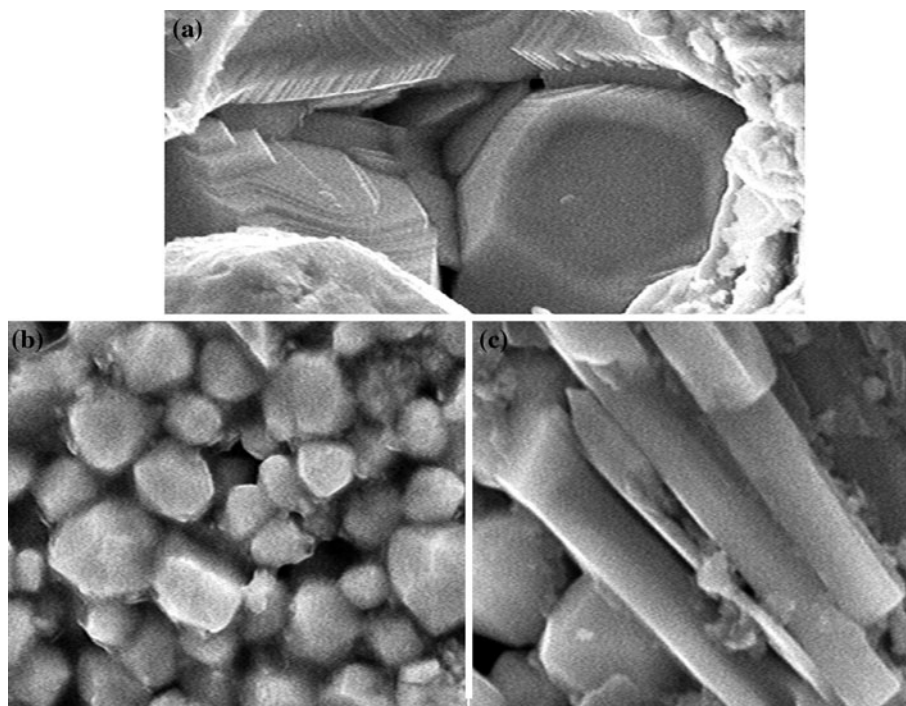


**Fig. 1** X-ray pattern at temperature 363 K of the BTZ-10 sample

**Fig. 2** SEM images of surface microstructure for BT **a** and BTZ30 **b**, **c** samples



## Results and discussion

Figure 1 presents the X-ray pattern for polycrystalline sample of BTZ10 at the temperature of PE–FE phase transition ( $T_m = 363$  K). It shows that at this temperature only 13% of the tetragonal phase ( $a = b = 4.003$  Å,  $c = 4.058$  Å) and 87% of the cubic phase ( $a = 4.031$  Å) exist.

This means that a 10% Zr concentration leads to freezing of the paraelectric, cubic structure. For BTZ30 only the cubic phase was observed at room temperature.

Figure 2 shows the SEM image of surface structure of pure BT (a) and BTZ30 (b, c) samples.

In this figure one can see crystallites with sharp edges of BT, the crystallites with smooth edges (b) and “micro-rollers” (c) of BTZ30.

Variety of crystallites (formed for high concentrations of Zr) follows from local gradients: of temperature and Zr ions concentration.

Figure 3 shows three clear maxima for the BT sample, involving the following structural phase transitions: C–T, T–O, O–R.

One can see a large increase of diffuseness of PT as well as a strong lowering of the  $T_m$  with increase of concentration of zirconium (see Fig. 4).

Figure 5 present the temperature changes of the real part of the electric permittivity  $\epsilon'(T)$  for BTZ20. The independence of the  $T_m$  on the frequency of the applied electric field pointed on the DPT.

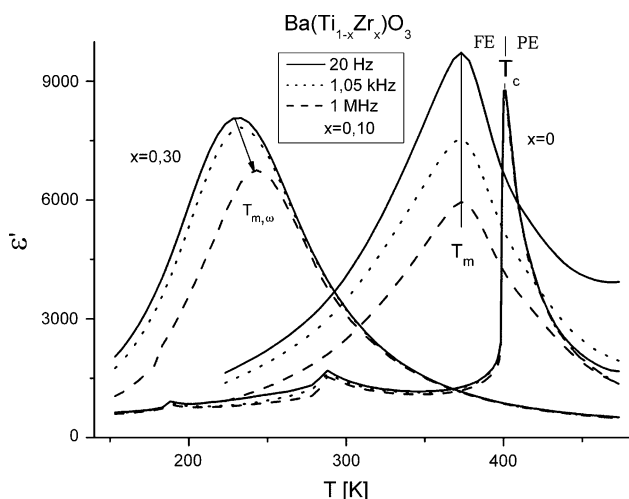


**Fig. 3** The real part of dielectric permittivity  $\epsilon'$  as a function of temperature for polycrystalline BTZx samples

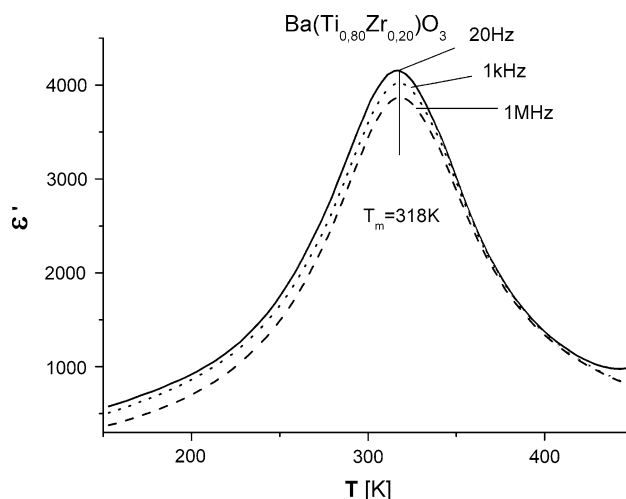


**Fig. 5** The real part of dielectric permittivity  $\epsilon'$  as a function of temperature for polycrystalline BTZ20 sample

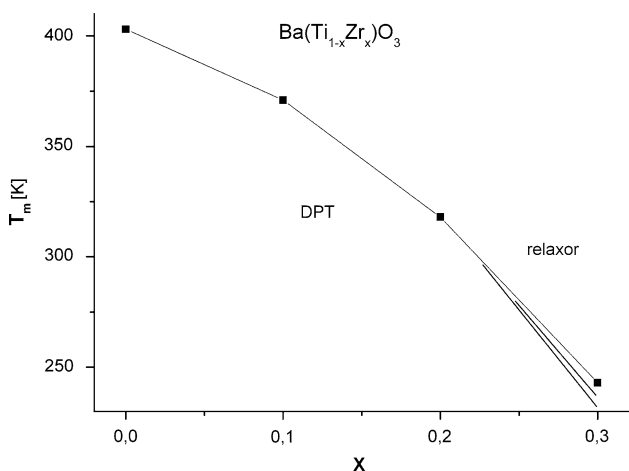


**Fig. 4** Temperature  $T_m$ , of maximum of the dielectric constant  $\epsilon'$  as a function of  $x$  concentration for polycrystalline BTZx samples

The following formula describes ferroelectric materials with DPT:

$$\epsilon^{-1} = \epsilon_m^{-1} + A(T - T_m)^\gamma, \tag{1}$$

where  $\epsilon_m$  is the maximum value of the electric permittivity  $\epsilon'$ ,  $A$ , and  $\gamma$  are fixed constants.

In DPT the value of  $\gamma$  is close to 2. These values were compiled in Fig. 6, where:

$$y = \epsilon^{-1} - \epsilon_m^{-1} \tag{2}$$

$$x = T - T_m. \tag{3}$$

Figure 3 shows a broad phase transition in BZT30. The PT is typical for relaxor materials.

From the glass model one can write the following Vogel-Fulcher equation [24, 25] involving  $T_{m,v}$  values for different frequencies:

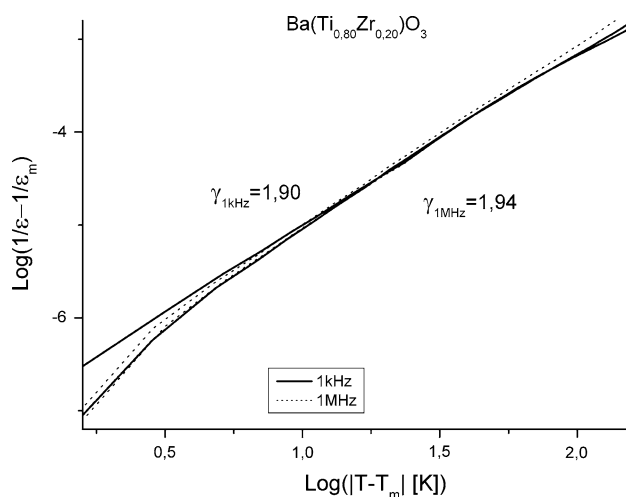


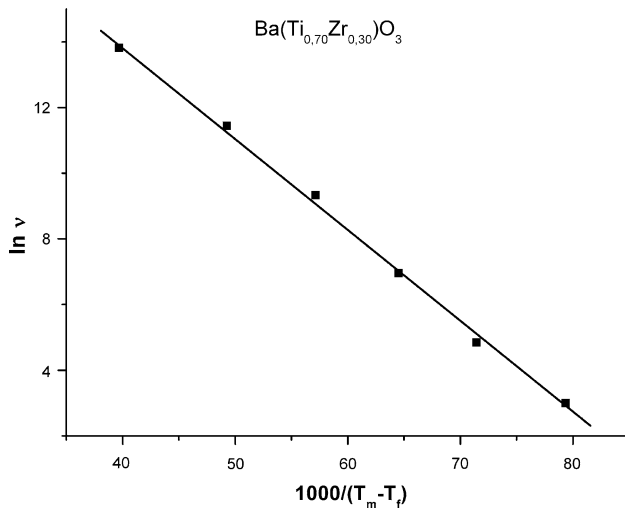
**Fig. 6** Dependence of  $(\log y)$  on  $(\log |x|)$  for polycrystalline BTZ20 sample

$$v = v_0 \exp\left(\frac{E_a}{k_B(T_{m,v} - T_f)}\right) \tag{4}$$

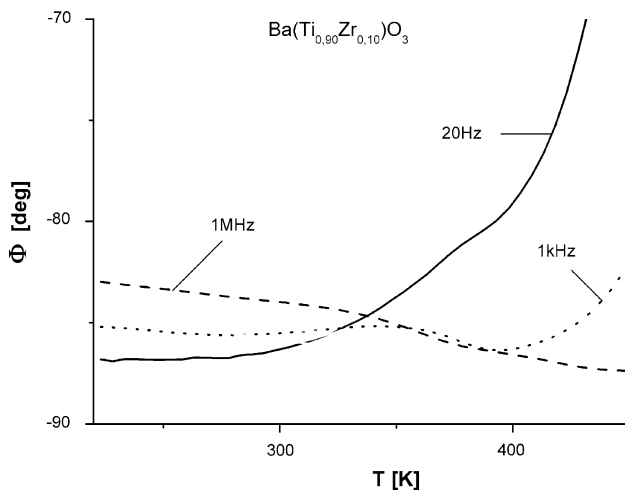
where  $v$  and  $v_0$  are the relaxation frequency at temperature  $T$  and a sufficiently high temperature, respectively,  $E_a$  is the activation energy of polar regions,  $k_B$  is the Boltzmann constant and  $T_f$  is the freezing temperature of polar regions.

Figure 7 present the dependence of  $(\ln v)$  on  $(1000/(T_{m,v} - T_f))$ . From this graph one can calculate a glassy temperature value:  $T_f \approx 140$  K.

Figures 8 and 9 show the value of phase angle as a function of temperature for concentrations  $x = 0.10$  and  $0.20$ . All  $\Phi$  values are close to approx.  $-80$  to  $-90^\circ$



**Fig. 7** Dependence of  $\ln \nu$  on  $(1000/(T_m - T_f))$  for polycrystalline, BTZ30 ( $T_f \approx 140$  K)



**Fig. 8** Dependence of  $\Phi$  on  $T$  for polycrystalline BTZ10

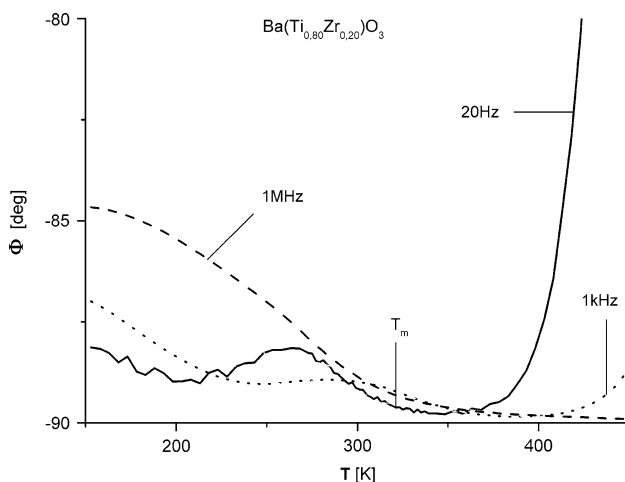


**Fig. 9** Dependence of  $\Phi$  on  $T$  for polycrystalline BTZ20

characteristic for the capacitive character of the material. This is also connected with the polar character of the material. Moreover, it is consistent with the occurrence of polar regions (clusters [26, 27]) in BTZx.

In PE–FE PT temperatures peaks of the phase angle were not observed. This suggests that the PT is not connected with structural PT but it follows from the change of the polar system in the region of PE–FE PT.

The change of system of these clusters, in the region of the PF phase transition, leads to formation of a strong maximum in measurements of the real part of the electric permittivity.

The clusters polarizability change with temperature is the source of dipolar polarization  $P_d$  [28–30]. This polarization originates from short-range interaction of electric dipoles. The growth of clusters size is a consequence of their long-range structural and electric collectivization.

## Conclusions

The study presents the results of the dielectric measurements of BTZx. They confirm that a substitution of Zr ions in sublattice B leads to strong diffuseness and to lowering of the temperature of PE–FE phase transition. In the room temperatures, the BTZx ( $0 < x < 0.20$ ) is ferroelectric. For  $0.10 < x < 0.20$  BTZ show DPT. For  $x \geq 0.30$  Zr ions lead to freezing of cubic structure below the temperature of the PE–FE phase transition. This behavior is similar to that of other relaxor type ferroelectrics.

The lack of structural phase transition at the temperature  $T_m$  for  $0.10 \leq x \leq 0.30$ , suggest that the PE–FE PT is connected solely with the change of clusters system polarizability.

The observed change of physical properties of BTZx can be applied in practice to change the work temperature of electromechanical devices.

**Open Access** This article is distributed under the terms of the Creative Commons Attribution Noncommercial License which permits any noncommercial use, distribution, and reproduction in any medium, provided the original author(s) and source are credited.

## References

1. Kajtoch C (1990) Doctor's thesis Martin-Luther-University Halle-Wittenberg
2. Antonelli E, Silva RS, Hernandes AC (2006) *Ferroelectrics* 334(1):75
3. Bera J, Rout SK (2005) *Mater Lett* 59(1):135
4. Rehrig P et al (1999) *J Appl Phys* 86(3):1657
5. Yu Z et al (2002) *J Appl Phys* 92(3):1489
6. Yu Z et al (2000) *Appl Phys Lett* 77:1535
7. Dobal PS et al (2001) *J Appl Phys* 89(12):8085
8. Yu Z, Guo R, Bhalla AS (2000) *J Appl Phys* 88(1):410

9. Hennings D et al (2006) *JACS* 65(11):539
10. Weber U, Hennings D et al (2004) *JACS* 84(4):759
11. Hafer Ch, Mayer R, Boetger U, Waser R (2004) *J Eur Ceram Soc* 246:1473
12. Nanakorn N, Jalupoom P, Vaneesorn N, Thanaboonsombut A (2008) *Ceram Int* 34:779
13. Moulson AJ, Herbert JM (1990) *Materials properties and applications*. Chapman and Hall, London
14. Heywang W (1961) *Solid State Electronics* 3:51
15. Jonker GH (1964) *Solid State Electronics* 7:895
16. Fu LX, Zhang LY, Yao X (2008) *J Electroceram* 21(1–4):561
17. Ravez J, Simon A (2001) *J Solid State Chem* 162:260
18. Bokov AA, Ye Z-G (2000) *Solid State Commun* 116:105
19. Jonscher AK (1983) *Dielectric relaxation in solids*. Chelsea Dielectric Press Ltd, London
20. Cross LE (1994) *Ferroelectrics* 151:305
21. Kajtoch C (1997) *Ferroelectrics* 192:335
22. Ravez J, Simon A (2000) *Physica Status Solidi (a)* 178:793
23. Kajtoch C (2009) *Ceram Int* 35:2993
24. Vogel H (1921) *Phys Z* 22:645
25. Fulcher GS (1925) *J Am Ceram Soc* 8:339
26. Comes R, Lambert M, Guinier A (1970) *Acta Crystall* A26:244
27. Kajtoch C (1900) *Ferroelectrics Lett* 25:81
28. Burns G, Dacol FH (1982) *Solid State Commun* 42:9
29. Kajtoch C (1995) *Ferroelectrics* 172:465
30. Burns G, Dacol FH (1990) *Ferroelectrics* 104:25